Journal of Biomedical Optics

BiomedicalOptics.SPIEDigitalLibrary.org

Microfluidic surface-enhanced Raman scattering sensor with monolithically integrated nanoporous gold disk arrays for rapid and label-free biomolecular detection

Ming Li
Fusheng Zhao
Jianbo Zeng
Ji Qi
Jing Lu
Wei-Chuan Shih

SPIE.

Microfluidic surface-enhanced Raman scattering sensor with monolithically integrated nanoporous gold disk arrays for rapid and label-free biomolecular detection

Ming Li, Fusheng Zhao, Jianbo Zeng, Ji Qi, Jing Lu, and Wei-Chuan Shih*
University of Houston, Department of Electrical and Computer Engineering, 4800 Calhoun Road, Room N308 Eng. Bldg. 1, Houston, Texas 77204, United States

Abstract. We present a microfluidic surface-enhanced Raman scattering (SERS) sensor for rapid and label-free biomolecular detection. Our sensor design mitigates a common limiting factor in microfluidic SERS sensors that utilize integrated nanostructures: low-efficiency transport of biomolecules to nanostructured surface which adversely impacts sensitivity. Our strategy is to increase the total usable nanostructured surface area, which provides more adsorption sites for biomolecules. Specifically, a nanoporous gold disk (NPGD) array, a highly effective SERS substrate, has been monolithically integrated inside a microfluidic chip. Individual NPGD is known to feature an order of magnitude larger surface area than its projected disk area. The increased surface area arises from nanoscale pores and ligaments three-dimensionally distributed in the NPGD, which manifest themselves as high-density SERS hot-spots. High-density NPGD arrays further guarantee large coverage of these hot-spots on the microchannel floor. The sensor performance has been demonstrated using Rhodamine 6G to quantify spatial uniformity and determine the shortest detection time. Next, the sensor is applied to detect two biomolecules, dopamine and urea, with unprecedented detection limit and speed compared to other existing microfluidic SERS sensors. The sensor holds great promise in point-of-care applications for various biomolecular detections. [DOI: 10.1117/1.JBO.19.11.111611]

Keywords: surface-enhanced Raman scattering; microfluidics; nanoporous gold disk; biomolecular sensing; dopamine; urea.

Paper 140129SSR received Feb. 28, 2014; revised manuscript received Jun. 7, 2014; accepted for publication Jun. 19, 2014; published online Jul. 23, 2014.

1 Introduction

Detection and identification of molecules in a rapid, sensitive, and cost-effective manner play an essential role in the point-of-care applications. Microfluidic platforms hold great promise in achieving this purpose due to their distinct advantages such as small sample and reagent consumption, fast reaction and analysis times, environmental and user friendliness, and low cost.[1,2] To date, a variety of methods have been developed and applied within microfluidic systems for molecular sensing, including electrochemical,[3–5] mechanical,[6,7] mass spectrometric,[8,9] and optical (i.e., fluorescence,[10] absorbance,[11] Raman spectroscopy,[12] surface plasmon resonance,[13] and chemiluminescence[14]) detection techniques. Among these available methodologies, surface-enhanced Raman scattering (SERS)-based detection techniques have attracted much attention because of their "fingerprinting" capability for label-free and multiplexed sensing.

SERS is a Raman spectroscopic technique where the Raman scattering is enhanced primarily by near-field electromagnetic enhancement due to localized surface plasmon resonance.[15–18] SERS enables label-free molecular detection and identification with high-sensitivity, high-specificity, and requires little or no sample preparation. With the advances in nanofabrication technologies and fundamental knowledge of plasmonics over the past decades, many SERS-based *in vitro* assays have been developed for various applications,[19] such as DNA hybridization,[20] immunoassay,[21] biosensing,[22] intracellular analyses,[23] extracellular imaging,[24] and cancer detection.[25] However, many existing assays require a great deal of sample preparation such as centrifugation, heating, mixing, and surface modification, which represent challenges for translation to microfluidic chips.

There are two main approaches for implementing SERS detection in microfluidic platforms. One is based on solution-phase colloidal metal nanoparticles acting as Raman enhancers, which interact with analytes of interest and adsorb them onto the surface via mixing before SERS measurements are conducted.[26,27] Choo's group[28,29] utilized a gradient microfluidic chip for SERS-based immunoassay of the alpha-fetoprotein model protein marker and detection of DNA oligonucleotides. Ackermann et al.[30] have employed a two-phase liquid/liquid segmented flow system in SERS detection, and the limit of detection (LOD) within the droplet was about 500 nM with an integration time of 1 s. In general, SERS intensities depend on the degree of colloid aggregation that is significantly influenced by sample properties such as ionic strength.[31] In order to improve SERS signals, colloid nanoparticles were effectively concentrated by geometrical barriers.[32,33] Adenine molecules lower than 10 pM were detected,[32] but this can be a relatively time-consuming process, because the sample was prepared by an activation agent (i.e., sodium chloride) to increase

*Address all correspondence to: Wei-Chuan Shih, E-mail: wshih@uh.edu

nanoparticle aggregation, and it takes 15 and 30 min aggregate nanoparticles into clusters and maintain a stable trapping effect on molecules, respectively.

Some of the issues for the colloidal nanoparticle approach are avoided in a nanostructure-based approach, and several nanostructured metal surfaces serving as SERS-active substrates in microfluidic platforms have been developed. The existing nanostructure-integrated microfluidic SERS sensors primarily use Ag, including arrays of nanowells,[34] nanopillars,[35] nanodomes,[36] nanograting,[37] nanoplates,[38] and nanodots.[39] Although Ag-based SERS substrates have inherently higher SERS effects compared to Au-based ones, the long-term stability is worse due to the gradual degradation of Ag surfaces. However, after an extensive literature search, we have only identified four papers describing microfluidic SERS sensors bearing immobilized Au-based nanostructures in the past 10 years.[31,36,40,41] Gold nanowell arrays,[31] fabricated by depositing a thin Au-film on a polystyrene (PS) nanosphere monolayer, were utilized for SERS measurement of urine. Although the LOD for key biomolecules (i.e., urea) was not reported, the paper demonstrated robust detection under various sample PH values, which significantly compromised the colloidal nanoparticle approach. Au-coated nanodome arrays[36] were applied to detect 25 mM urea in solutions. Gamby et al.[40] reported gold nanowires synthesized in a polycarbonate microchannel by an electrocrystallization technique as an SERS-active device, and isonicotinic acid (10 μM) in perchloric acid (1 mM) was detected. Also, gold nanoparticles[41] were deposited in microchannels by laser electrodispersion, and SERS measurement was conducted for 0.1 μM crystal violet (CV) in a continuous flow. We note that Au-coated Ag bimetallic nanoparticles as SERS substrates show higher signal enhancement and biocompatibility than the monometallic Ag nanoparticles,[42,43] but there are no reports regarding the integration of bimetallic substrates in microfluidics yet.

Among the existing demonstrations of microfluidic SERS sensors with immobilized metal nanostructures, the selection of target molecules is very limited. To date, a small set of model compounds has been commonly employed such as dye molecules (R6G, CV) and high surface affinity molecules such as thiols and adenine. Dye molecules typically have light absorption features which provide additional enhancement that is not available for nonabsorbing species; thiols are known to strongly bind Au and Ag; adenine is known to exhibit an excellent SERS signal with the detection limit easily in the nanomolar range. As such, it should be recognized that sensor performance on practical target biomolecules cannot be simply guaranteed by these testing results. Rather, effective detection of a broader range of biomolecules needs to be established in a case by case fashion. Indeed, using urea detection as an example, the only quantitative result we have identified on microfluidic SERS using Au-coated nanodome arrays was previously mentioned.[36]

Although the nanostructured surface approach typically provides better robustness against sample conditions, the amount of molecules that can effectively interact with the nanostructures is quite limited by diffusion—as low as <1% can be estimated using a simple boundary layer analysis in a largely laminar flow situation.[44] We note that the colloidal nanoparticle approach, in contrast, can achieve much thorough mixing either outside or inside microchannels.

To address the diffusion limit mentioned above, our strategy is to increase the total usable area of the nanostructured surface, which provides more adsorption sites for biomolecules. Our group has developed nanoporous gold disks (NPGDs) with large specific areas, high-density plasmonic hot-spots, high SERS enhancement factor ($> 10^8$), high photothermal conversion efficiency, and effective SERS by contact stamping and in microfluidics.[45–49] The total surface area of our NPGD substrate is about 20-fold that of the solid gold disk substrate, and the effective roughness factor (the ratio of the chemically active surface area to the geometrical surface area) lies in between 7.4 and 20,[45] which would provide a promising platform to meet the needs. To our knowledge, this is the first implementation of nanoporous gold and related materials monolithically integrated inside a microfluidic chip for increased plasmonic surface area.

In the following, we first outline the design and fabrication process of our sensor. Next, we demonstrate sensor robustness and uniformity using R6G molecules of concentrations ranging from 1 μM to 1 mM in aqueous solutions. We subsequently show unprecedented performance for detecting and identifying different biomolecules, including dopamine (DA, a major neurotransmitter in the central nervous system) and urea (a physiological metabolite).

2 Materials and Methods

2.1 *Fabrication of the Microfluidic SERS Sensor*

Figure 1 schematically illustrates the fabrication process for our sensor, which is accomplished by oxygen-plasma bonding of

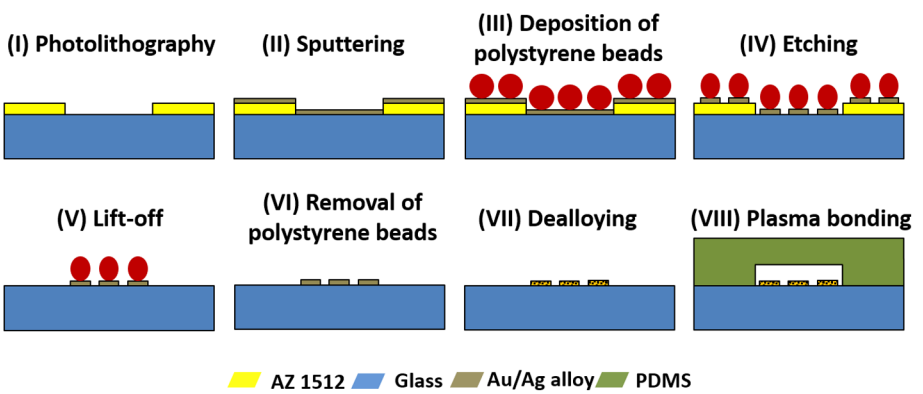

Fig. 1 Schematic view of the fabrication process for the surface-enhanced Raman scattering (SERS)-active nanoporous gold disk (NPGD) arrays within a microfluidic channel (diagram not to scale).

two constructs: an SERS-active glass substrate with patterned NPGD arrays and a polydimethylsiloxmane (PDMS) layer containing a microfluidic network. The overall fabrication process includes a single low-cost transparency mask and four major steps: (a) definition of the SERS detection area, (b) construction of the NPGD arrays, (c) patterning of the microfluidic channel, and (d) plasma bonding.

2.1.1 *Definition of SERS sensing area*

The first step produces a confined SERS detection area within the microchannel network, in which a photoresist mold containing microchannel structures are built using standard photolithography techniques. Positive photoresist (AZ 1512, MicroChem Corp., Newton, Massachusetts) was spun on a clean glass coverslip by a two-step coating cycle (500 rpm for 5 s and 3000 rpm for 45 s), producing a nominally 1-μm thick film. After a pre-bake at 95°C for 4 min, the photoresist film was exposed to UV light (MA6, Karl Suss, Sunnyvale, California) with 350 mJ/cm^2 through a transparency mask (Pageworks, Cambridge, Massachusetts) having the structures of the desired microchannel network. The coverslip was then gently vibrated in the developer solution for around 30 s to dissolve the exposed area of the photoresist, leaving a negative relief containing the microchannel network (I). After that, the coverslip was rinsed thoroughly with deionized (DI) water and blow-dried by nitrogen gas.

2.1.2 *Construction of NPGD arrays*

In this step, SERS-active NPGD arrays are fabricated within the predefined region for SERS detection by generic nanosphere lithography.[50] Briefly, the process started by coating a 120-nm thick alloy layer (Ag/Au atomic ratio 82.5:17.5, $Ag_{82.5}Au_{17.5}$) by sputtering on the glass coverslip with the patterned microchannel structures from Sec. 2.1.1. After depositing a self-assembled monolayer (SAM) of closely-packed PS beads of 600-nm diameter onto the surface serving as masks (III), the coverslip was treated with two steps of plasma etching (IV): oxygen etching to shrink PS beads, and argon reactive ion etching to etch away the portion of alloy film unmasked by the PS beads, which led to high fill-factor (~50% coverage) alloy disk arrays underneath the PS bead monolayer. A lift-off process was then conducted to remove the photoresist and all the nanostructures on its surface (V), leaving only alloy disks and PS residues within the predefined SERS detection region. After removing the PS residues (VI) by sonication in chloroform for 1 min, and dealloying of silver (VII) in concentrated nitric acid for 1 min, NPGD arrays with the designed geometry were formed on the coverslip. Due to the internal nanoporous network, the fabricated NPGDs have a large specific surface area for molecular adsorption sites, and high-density plasmonic hot-spots for SERS measurement.

2.1.3 *Patterning of matching microfluidic channel*

The polydimethylsiloxane (PDMS) microfluidic channel was fabricated using a standard soft lithography technique. Detailed information on this procedure can be found in our previous work.[51] SU-8 negative photoresist was first patterned using a standard photolithography technique to create a positive relief of the microchannel pattern on the surface of a silicon wafer. The pattern of the microfluidic network was designed to match the SERS detection region on the coverslip. Thus, the same transparent mask used previously was employed here. Then, liquid PDMS (Sylgard 184, Dow Corning, Midland, Michigan) prepared by mixing a base and curing agent at a weight ratio of 10:1 was poured over the master, degassed, and cured in a vacuum oven at 80°C for 2 h. The negative PDMS cast with the microchannel pattern was then peeled off the master, and two via-holes were punched for fluidic access.

2.1.4 *Oxygen-plasma bonding*

The bonding step was finally carried out to form enclosed microchannels covered by NPGD arrays. The top surface of the prepared coverslip with NPGD arrays and the microchannel side of the PDMS layer were treated by oxygen plasma for 2 min with a pressure and a power of 200 mTorr and 100 W, respectively. After that, both surfaces were covered with methanol acting as a lubricant, and were precisely aligned under a microscope for face-to-face contact. After heating at 90°C for 5 min, two substrates were firmly bonded together producing the final sensor (VIII).

A schematic of the preassembled sensor is shown in Fig. 2(a), and Fig. 2(b) shows a visual image of the final sensor utilized in our experiment. When red R6G solution was injected into the SERS-active microchannel, no leakage was observed [see Fig. 2(c)], which indicates the interconnectivity and transparency of the microchannel. The height, width, and length of the microchannel were 20 μm, 20 μm, and 1 cm, respectively.

As shown in Fig. 3, scanning electron microscopy images were acquired to show the structure of the fabricated NPGD arrays and an individual disk. The average diameter, thickness, and pore size of the disks were ~400, 75, and 14 nm, respectively.

2.2 *SERS Measurements*

In our experiment, SERS measurements were carried out using a home-built line-scan Raman microscopy system, where the

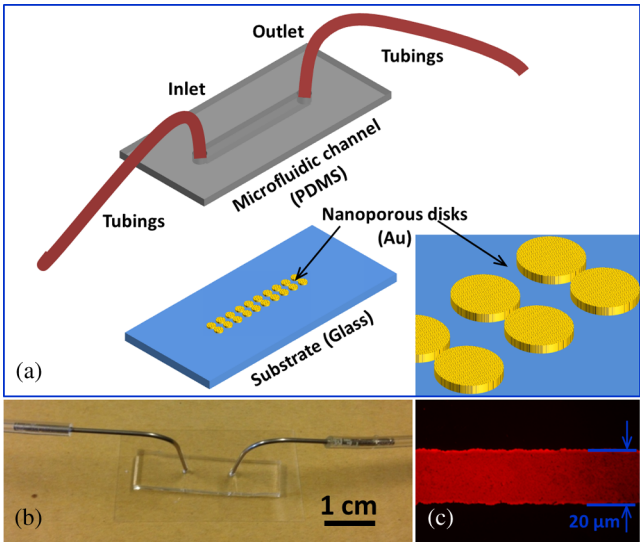

Fig. 2 Schematic illustration of the sensor architecture: (a) preassembled parts consisting of the NPGD arrays coverslip and the polydimethylsiloxmane microchannel network. The inset at the corner is an enlarged diagram showing the NPGDs; (b) a visual image of the final sensor used in experiments; (c) a fluorescence microscopic image of the microchannel filled with R6G solution to confirm properly sealed microchannels.

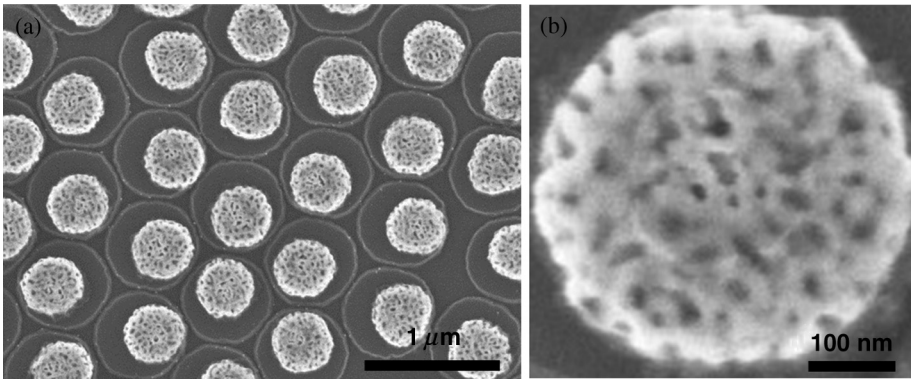

Fig. 3 Scanning electron microscopy images: (a) NPGD arrays and (b) a single NPG disk.

excitation laser was shaped into a 1×133 μm^2 line at the sample plane. Spatially resolved Raman spectra from the entire line can be recorded by a spectrograph charge-coupled device system (LS-785, Princeton Instruments, Acton, Massachusetts). In other words, a single-shot spectral image from a region of 1×133 μm^2 can be recorded over the range from 250 to 1800 cm^{-1}, with a spatial resolution of about 1 μm and a spectral resolution of 8 cm^{-1}.[52,53] The excitation laser wavelength was 785 nm with 28 mW at the sample. The laser line was focused within the microchannel and scanned for area mapping, and the corresponding SERS spectra were recorded by a computer with WinSpec software (PIActon), followed by background removal in MATLAB (Mathworks, Natick, Massachusetts) using automated polynomial-based techniques.[54,55] Rhodamine 6G (R6G), DA, and urea in powder form were purchased from Sigma-Aldrich (St. Louis, Missouri). Pure stock solutions of individual molecules were prepared by dissolving the powders in DI water, and were further diluted to make different concentrations. The sample solutions were introduced into the sensor for measurement via tubing connected to a syringe controlled by a syringe pump (Fusion 100, Chemyx Corporation, Stafford, Texas).

2.3 *Calculation of EF*

In order to evaluate the enhancement capability of our sensor, the EF was calculated using the formula as follows:[56]

$$\mathrm{EF} = \frac{I_{\mathrm{SERS}} \cdot N_{\mathrm{ref}}}{I_{\mathrm{ref}} \cdot N_{\mathrm{SERS}}},$$

where I_{SERS} and I_{ref} are the Raman intensity from our sensor and a reference measurement from either a bulk sample or a commercial SERS substrate (Klarite, Renishaw), respectively. N_{SERS} and N_{ref} are the number of molecules contributing to the corresponding Raman intensity. Benzenethiol (BT) was selected as a maker for the EF measurement due to its capability to form an SAM on gold or silver surfaces with a known density, which facilitates the estimate of the number of molecules. In addition, BT lacks absorption features near the excitation laser wavelength (785 nm), thus avoiding any confounding effects of molecular resonance or preresonance not due to plasmonics. The EF was determined by using the peak intensity at 1575 cm^{-1} for SERS measurements from our sensor and Klarite, and 1584 cm^{-1} as the normal for the Raman spectrum from the bulk sample. More details can be found in our previous work.[45] The result indicates that our sensor has an enhancement of at least 10^6. We note that this value is considerably lower than that in our previous work, possibly due to the combined effects of the oxygen-plasma/methanol treatment for bonding, the differences in NPGD size and pore size, and the lack of an underlying gold adhesion layer. Future work is needed to identify the actual cause.

3 Results and Discussion

3.1 *Characterization of Spatial-Uniformity of the Microfluidic SERS Sensor*

R6G solution of 1 mM concentration was loaded into a syringe and then injected into the sensor. After the microchannel was filled with the solution for 10 min, SERS spectra were acquired from different locations with 10 s acquisition time each. Figure 4(a) shows SERS signals from 10 different locations within one sensor, where dominant SERS peaks corresponding to R6G, i.e., 611, 773, 1130, 1193, 1315, 1366, 1512, 1603, and 1647 cm^{-1} (Ref. 57) are identified. The relative intensity variations of major R6G peaks were calculated to be within 8% to −8% of the average intensity as shown in Fig. 4(b), indicating the high uniformity and reproducibility of our sensor. We have also evaluated the SERS intensity uniformity across devices and found a similar range of variations. This level of variations agrees well with our previous work. The good uniformity is attributed to the highly uniform NPGD arrays within the microchannel. Our sensor uniformity is slightly better than recent results published in Small 2014, which reported a range from −13% to +13%.[35] To validate that the spectra measured were indeed SERS and not normal Raman scattering, we have performed similar measurements inside the same microchannel but without the NPGD arrays. As shown in Fig. 4(c), very little normal Raman scattering signal was observed from the microchannel without the NPGD arrays, thus confirming all our measurements were indeed SERS.

3.2 *SERS Detection of R6G with Different Concentrations*

To further assess the sensing capability of the sensor, SERS measurements were performed for R6G solutions of different concentrations at 1, 10, 100, 200, 500, and 1000 μM. The measurement for each R6G concentration was performed five times at five different locations 10 min after injecting the sample into the sensor. Figure 5 shows the averaged SERS spectra for different concentrations of R6G. The characteristic peaks of R6G are

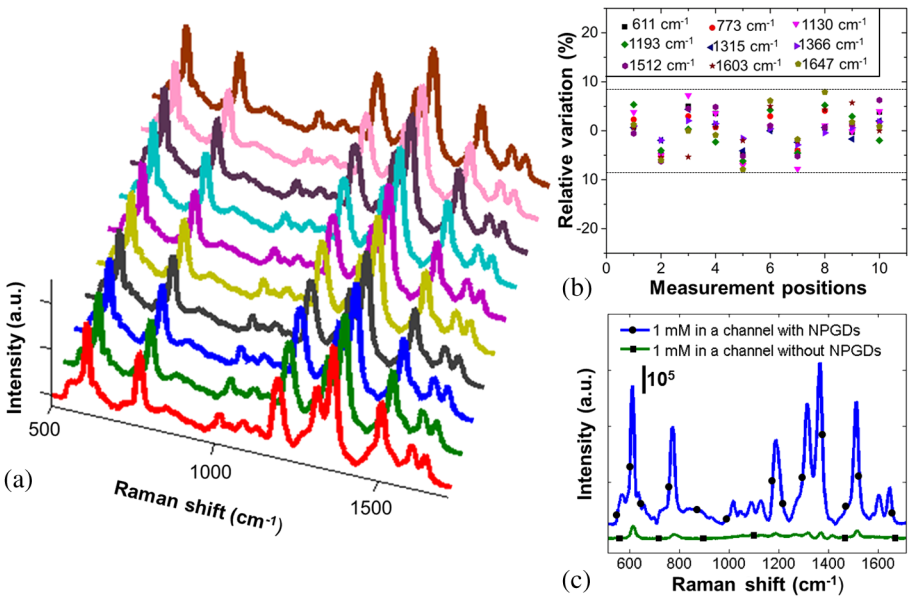

Fig. 4 R6G measurements: (a) SERS spectra of 1 mM R6G detected in the SERS-active microfluidic channel at 10 different locations; (b) relative intensity variations of major peaks for the 10 locations; (c) spectra comparison of 1 mM R6G in a microchannel with NPGDs and a microchannel without NPGDs (as reference).

clearly identified in all spectra, and the peak intensity increased with increasing R6G concentration. To further demonstrate the performance, the intensity variations of the 1366 cm^{-1} peak were used for quantitative evaluation. As shown in the inset, a highly correlated intensity-concentration relationship is obtained from 1 μM to 1 mM. The error bars represent the standard deviation from five measurements. The LOD is defined as the concentration at which the Raman intensity value is equal to the averaged blank intensity at 1366 cm^{-1} plus three times the standard deviation, which was calculated to be 5.16 nM using the calibration curve. Again, the normal Raman spectra of 1 mM R6G in a microchannel without NPGDs was also presented for comparison (black line).

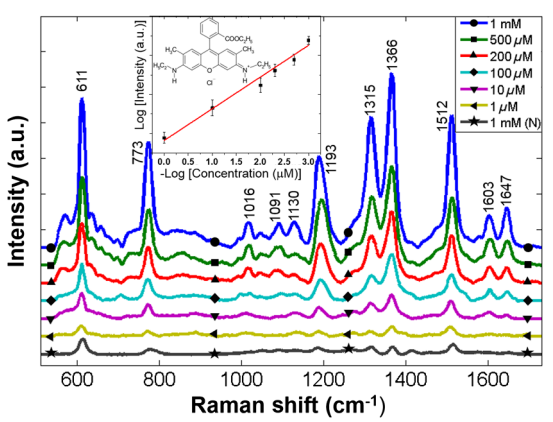

Fig. 5 Concentration-dependent SERS spectra of R6G measured in the sensor. The concentration ranges from 1 μM to 1 mM. The bottom trace was acquired from 1 mM R6G inside a microchannel without NPGD arrays. The inset indicates the variations of R6G peak intensity at 1366 cm^{-1} as a function of R6G concentration along with the molecular structure of R6G. The error bars represent the standard deviation from five measurements.

3.3 *SERS Detection of R6G with Continuous Flow*

In addition to investigating the performance of the sensor without flow, its behavior under continuous flow was also studied. R6G solution at 100 μM was loaded into a syringe and injected into the sensor via a syringe pump at a flow rate of 3 μL/ min. SERS measurements were taken *in situ* under the continuous-flow condition with an integration time of 2 s per acquisition. Figure 6 shows the intensity variations corresponding to the 1366 cm^{-1} peak within the first minute. The starting point (i.e., $t = 0$ s) indicates the initial situation, where the NPGD arrays in the SERS detection region were not yet flooded by the sample solution. It is found that the signal intensity rapidly increased within the first 10 s, then steadily and slowly increased in the time range from 10 to 45 s, reaching a saturation limit in the last 10 s. After injecting the solution into the channel for

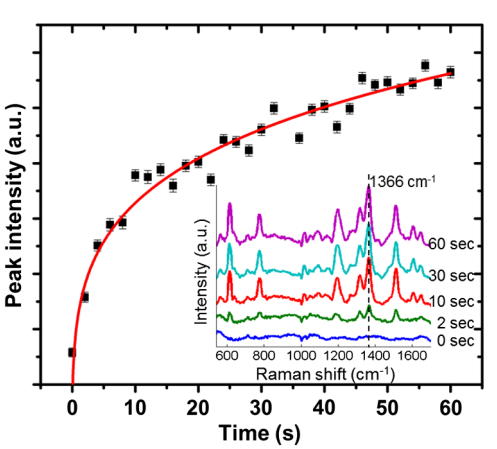

Fig. 6 Intensity variations versus time under the continuous-flow condition. The 1366 cm^{-1} peak intensity of 100 μM R6G was plotted. The inset presents the measured SERS spectra at five selected time points of 0, 2, 10, 30, and 60 s.

1 min, only small signal intensity variations (<10%) were observed, indicating the stability and robustness of SERS detection in continuous-flow measurement. The dynamic behavior can be interpreted as below. When more and more R6G molecules were adsorbed onto the surface of the NPGD arrays, the SERS intensity kept increasing within the first minute. The intensity reached a quasiplateau when maximum numbers of R6G molecules were adsorbed at a fixed flow rate. Further, the intensity achieved around 70% of that at the quasiplateau state within the first 10 s. The result suggests that the sensor can provide rapid detection (i.e., <2 s) in solutions.

3.4 *SERS Detection of DA with Different Concentrations*

Next, we demonstrate that our sensor can detect DA, an essential neurotransmitter playing the role of controlling the brain's reward and pleasure centers. DA solutions of different concentrations ranging from 100 nM to 7.5 μM were introduced into the sensor by a syringe. After filling the microchannel for 10 min, the SERS spectra of DA molecules were measured at five locations with 30 s acquisition time each. The averaged spectra are shown in Fig. 7, where major SERS peaks of DA at 590, 632, 815, 961, 1152, 1272, 1327, and 1486 cm^{-1} (Ref. 58) are clearly identified. A good linear relationship is observed by plotting the SERS intensity at 1272 cm^{-1} versus concentrations as shown in the inset, and the LOD was calculated to be 32.4 nM. The black line represents the Raman spectra of 7.5 μM DA in a microchannel without NPGD arrays where no peaks were observed, thus validating the measured spectra were indeed SERS. Compared to the results of detecting DA in a mixer with SERS-active Ag nanodots published in Lab on a Chip 2014,[39] our spectra exhibited a significantly better signal-to-noise ratio at the higher concentration (100 μM).

3.5 *SERS Detection of Urea at Physiological Concentrations*

In addition to a neurotransmitter, we also measured urea at physiological concentrations from 1 to 20 mM (Ref. 36) in artificial urine, which was prepared using 10.0 g of sodium chloride, 6.0 g of potassium, chloride 6.4 g of sodium phosphate (monobasic, monohydrate) dissolved in 1 L of DI water. Urea is a primary nitrogen-containing compound and a key metabolic indicator in urine. The corresponding SERS spectra are shown in Fig. 8. The major peak near 1000 cm^{-1} is identified, which corresponds to the symmetrical C-N stretching vibration mode.[59] A good linear relationship is observed by plotting the SERS intensity at 1001 cm^{-1} versus concentrations as shown in the inset, and the LOD was calculated to be 0.67 mM with a power density of 0.21 mW/μm^2 and integration time of 10 s. The Raman spectra of 20 mM urea in a microchannel without NPGD arrays are also presented (bottom black line), where no Raman signal of urea is detected. Compared to the results of urea detection by Au-coated nanodome arrays recently published in Small,[36] our sensor has achieved a lower detection limit. The results suggest that our sensor provides a promising and versatile capability for clinical and diagnostic applications, such as kidney function monitoring and urine analysis.

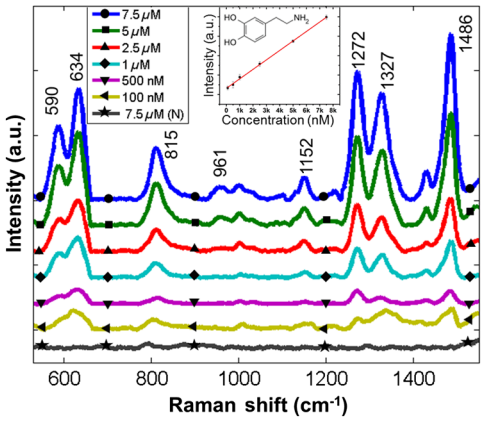

Fig. 7 Concentration-dependent SERS spectra of dopamine (DA) in the sensor. Five selected concentrations ranging from 100 nM to 7.5 μM were used with an acquisition time of 30 s each. The bottom trace was acquired from 100 μM DA inside a microchannel without NPGD arrays. The inset shows the intensity variations at 1272 cm^{-1} with respect to DA concentration along with the molecular structure of DA. The error bars represent the standard deviation from five measurements.

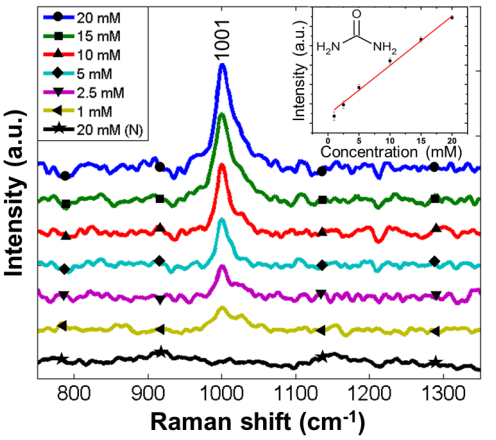

Fig. 8 Concentration-dependent SERS spectra of urea in the sensor. Five selected concentrations ranging from 1 to 20 mM were used with an acquisition time of 10 s each. The bottom trace was acquired from 20 mM urea inside a microchannel without NPGD arrays. The inset shows the intensity variations at 1001 cm^{-1} with respect to urea concentration along with the molecular structure of urea.

4 Conclusions

In conclusion, we have developed a rapid (i.e., <2 s) and label-free microfluidic SERS sensor with monolithically integrated NPGD arrays. The SERS-active NPGD arrays exhibit a useful and reproducible EF of more than 10^6, and the capability for highly reproducible SERS measurements with relative intensity variations from 8% to −8%. R6G solutions in the concentrations ranging from 1 μM to 1 mM have been detected and quantitatively evaluated, and the performance of the sensor in continuous-flow conditions has been assessed. Moreover, the sensor's capabilities have been studied by detecting and identifying a neurotransmitter (DA), and a physiological metabolite (urea), and the results show the lower detection limit compared to the best results from most recent works using an integrated nanostructured surface inside microchannels. We expect that the sensor would be applicable for detecting, identifying, and quantifying biomolecules for point-of-care application, e.g., urine screening and kidney function monitoring.

Acknowledgments

W.C.S. acknowledges funding from NSF CAREER Award (CBET-1151154), NASA Early Career Faculty Grant (NNX12AQ44G), and Gulf of Mexico Research Initiative Grant (GoMRI-030).

References

1. S. Haeberle and R. Zengerle, "Microfluidic platforms for lab-on-a-chip applications," *Lab Chip* **7**(9), 1094–1110 (2007).
2. D. Mark et al., "Microfluidic lab-on-a-chip platforms: requirements, characteristics and applications," *Chem. Soc. Rev.* **39**(3), 1153–1182 (2010).
3. K. Hayashi et al., "Development of nanoscale interdigitated array electrode as electrochemical sensor platform for highly sensitive detection of biomolecules," *J. Electrochem. Soc.* **155**(9), J240–J243 (2008).
4. Q. Kang et al., "Reduction of the impedance of a contactless conductivity detector for microchip capillary electrophoresis: compensation of the electrode impedance by addition of a series inductance from a piezoelectric quartz crystal," *Anal. Chem.* **80**(20), 7826–7832 (2008).
5. A. G. Crevillén et al., "Food analysis on microfluidic devices using ultrasensitive carbon nanotubes detectors," *Anal. Chem.* **79**(19), 7408–7415 (2007).
6. C. Ricciardi et al., "Integration of microfluidic and cantilever technology for biosensing application in liquid environment," *Biosens. Bioelectron.* **26**(4), 1565–1570 (2010).
7. K. Zhang et al., "A microfluidic system with surface modified piezoelectric sensor for trapping and detection of cancer cells," *Biosens. Bioelectron.* **26**(2), 935–939 (2010).
8. W. Kim et al., "Microfabricated monolithic multinozzle emitters for nanoelectrospray mass spectrometry," *Anal. Chem.* **79**(10), 3703–3707 (2007).
9. S.-H. Lee et al., "An integrated microfluidic chip for the analysis of biochemical reactions by MALDI mass spectrometry," *Biomed. Microdevices* **10**(1), 1–9 (2008).
10. M. Foquet et al., "Focal volume confinement by submicrometer-sized fluidic channels," *Anal. Chem.* **76**(6), 1618–1626 (2004).
11. Q. Mao and J. Pawliszyn, "Demonstration of isoelectric focusing on an etched quartz chip with UV absorption imaging detection[dagger]," *Analyst* **124**(5), 637–641 (1999).
12. P. C. Ashok et al., "Waveguide confined Raman spectroscopy for microfluidic interrogation," *Lab Chip* **11**(7), 1262–1270 (2011).
13. Y. Zhang et al., "Towards a high-throughput label-free detection system combining localized-surface plasmon resonance and microfluidics," *Lab Chip* **12**(17), 3012–3015 (2012).
14. J. L. Delaney et al., "Electrogenerated chemiluminescence detection in paper-based microfluidic sensors," *Anal. Chem.* **83**(4), 1300–1306 (2011).
15. M. Fleischmann, P. J. Hendra, and A. J. McQuillan, "Raman spectra of pyridine adsorbed at a silver electrode," *Chem. Phys. Lett.* **26**(2), 163–166 (1974).
16. C. L. Haynes, A. D. McFarland, and R. P. Van Duyne, "Surface-enhanced Raman spectroscopy," *Anal. Chem.* **77**(17), 338A–346A (2005).
17. J. N. Anker et al., "Biosensing with plasmonic nanosensors," *Nat. Mater.* **7**(6), 442–453 (2008).
18. J. P. Camden et al., "Controlled plasmonic nanostructures for surface-enhanced spectroscopy and sensing," *Acc. Chem. Res.* **41**(12), 1653–1661 (2008).
19. K. Hering et al., "SERS: a versatile tool in chemical and biochemical diagnostics," *Anal. Bioanal. Chem.* **390**(1), 113–124 (2008).
20. A. Barhoumi and N. J. Halas, "Label-free detection of DNA hybridization using surface enhanced Raman spectroscopy," *J. Am. Chem. Soc.* **132**(37), 12792–12793 (2010).
21. D. S. Grubisha et al., "Femtomolar detection of prostate-specific antigen: an immunoassay based on surface-enhanced Raman scattering and immunogold labels," *Anal. Chem.* **75**(21), 5936–5943 (2003).
22. K. C. Bantz et al., "Recent progress in SERS biosensing," *Phys. Chem. Chem. Phys.* **13**(24), 11551–11567 (2011).
23. I. Chourpa et al., "Intracellular applications of analytical SERS spectroscopy and multispectral imaging," *Chem. Soc. Rev.* **37**(5), 993–1000 (2008).
24. S. Preciado-Flores et al., "SERS spectroscopy and SERS imaging of Shewanella oneidensis using silver nanoparticles and nanowires," *Chem. Commun.* **47**(14), 4129–4131 (2011).
25. S. Y. Feng et al., "Nasopharyngeal cancer detection based on blood plasma surface-enhanced Raman spectroscopy and multivariate analysis," *Biosens. Bioelectron.* **25**(11), 2414–2419 (2010).
26. K. R. Strehle et al., "A reproducible surface-enhanced Raman spectroscopy approach. online SERS measurements in a segmented microfluidic system," *Anal. Chem.* **79**(4), 1542–1547 (2007).
27. L. X. Quang et al., "A portable surface-enhanced Raman scattering sensor integrated with a lab-on-a-chip for field analysis," *Lab Chip* **8**(12), 2214–2219 (2008).
28. N. Choi et al., "Simultaneous detection of duplex DNA oligonucleotides using a SERS-based micro-network gradient chip," *Lab Chip* **12**(24), 5160–5167 (2012).
29. M. Lee et al., "SERS-based immunoassay using a gold array-embedded gradient microfluidic chip," *Lab Chip* **12**(19), 3720–3727 (2012).
30. K. R. Ackermann, T. Henkel, and J. Popp, "Quantitative online detection of low-concentrated drugs via a SERS microfluidic system," *ChemPhysChem* **8**(18), 2665–2670 (2007).
31. K. W. Kho et al., "Polymer-based microfluidics with surface-enhanced Raman-spectroscopy-active periodic metal nanostructures for biofluid analysis," *J. Biomed. Opt.* **13**(5), 054026 (2008).
32. M. Wang et al., "An optofluidic device for surface enhanced Raman spectroscopy," *Lab Chip* **7**(5), 630–632 (2007).
33. S. H. Yazdi and I. M. White, "A nanoporous optofluidic microsystem for highly sensitive and repeatable surface enhanced Raman spectroscopy detection," *Biomicrofluidics* **6**(1), 014105 (2012).
34. G. L. Liu and L. P. Lee, "Nanowell surface enhanced Raman scattering arrays fabricated by soft-lithography for label-free biomolecular detections in integrated microfluidics," *Appl. Phys. Lett.* **87**(7), 074101 (2005).
35. H. Mao et al., "Microfluidic surface-enhanced Raman scattering sensors based on nanopillar forests realized by an oxygen-plasma-stripping-of-photoresist technique," *Small* **10**(1), 127–134 (2014).
36. H.-Y. Wu, C. J. Choi, and B. T. Cunningham, "Plasmonic nanogap-enhanced Raman scattering using a resonant nanodome array," *Small* **8**(18), 2878–2885 (2012).
37. B.-B. Xu et al., "A SERS-active microfluidic device with tunable surface plasmon resonances," *Electrophoresis* **32**(23), 3378–3384 (2011).
38. B.-B. Xu et al., "Localized flexible integration of high-efficiency surface enhanced Raman scattering (SERS) monitors into microfluidic channels," *Lab Chip* **11**(19), 3347–3351 (2011).
39. Y.-J. Oh and K.-H. Jeong, "Optofluidic SERS chip with plasmonic nanoprobes self-aligned along microfluidic channels," *Lab Chip* **14**(5), 865–868 (2014).
40. J. Gamby et al., "Polycarbonate microchannel network with carpet of Gold NanoWires as SERS-active device," *Lab Chip* **9**(12), 1806–1808 (2009).
41. V. Sans et al., "SE(R)RS devices fabricated by a laser electrodispersion method," *Analyst* **136**(16), 3295–3302 (2011).
42. A. Sivanesan et al., "Nanostructured silver-gold bimetallic SERS substrates for selective identification of bacteria in human blood," *Analyst* **139**(5), 1037–1043 (2014).
43. Y. Yang et al., "Preparation of Au-Ag, Ag-Au core-shell bimetallic nanoparticles for surface-enhanced Raman scattering," *Scr. Mater.* **58**(10), 862–865 (2008).
44. K. C. Dee, D. A. Puleo, and R. Bizios, *An Introduction to Tissue-Biomaterial Interactions*, John Wiley and Sons, Hoboken, New Jersey (2003).
45. J. Qi et al., "Surface-enhanced Raman spectroscopy with monolithic nanoporous gold disk substrates," *Nanoscale* **5**(10), 4105–4109 (2013).
46. G. M. Santos et al., "Characterization of nanoporous gold disks for photothermal light harvesting and light-gated molecular release," *Nanoscale* **6**(11), 5718–5724 (2014).
47. M. Li et al., "Stamping surface-enhanced Raman spectroscopy for label-free, multiplexed, molecular sensing and imaging," *J. Biomed. Opt.* **19**(11), 050501 (2014).
48. F. Zhao et al., "Monolithic NPG nanoparticles with large surface area, tunable plasmonics, and high-density internal hot-spots," *Nanoscale* **6**(14), 8199–8207 (2014).

49. J. Qi et al., "Label-free, *in situ* SERS monitoring of individual DNA hybridization in microfluidics," *Nanoscale* **6**(15), 8521–8526 (2014).
50. C. L. Haynes and R. P. Van Duyne, "Nanosphere lithography: a versatile nanofabrication tool for studies of size-dependent nanoparticle optics," *J. Phys. Chem. B* **105**(24), 5599–5611 (2001).
51. L. Ming et al., "Continuous particle focusing in a waved microchannel using negative dc dielectrophoresis," *J. Micromech. Microeng.* **22**(9), 095001 (2012).
52. J. Qi and W.-C. Shih, "Parallel Raman microspectroscopy using programmable multipoint illumination," *Opt. Lett.* **37**(8), 1289–1291 (2012).
53. J. Qi and W.-C. Shih, "Performance of line-scan Raman microscopy for high-throughput chemical imaging of cell population," *Appl. Opt.* **53**(13), 2881–2885 (2014).
54. J. Qi, J. Li, and W.-C. Shih, "High-speed hyperspectral Raman imaging for label-free compositional microanalysis," *Biomed. Opt. Express* **4**(11), 2376–2382 (2013).
55. C. A. Lieber and A. Mahadevan-Jansen, "Automated method for subtraction of fluorescence from biological Raman spectra," *Appl. Spectrosc.* **57**(11), 1363–1367 (2003).
56. E. C. Le Ru et al., "Surface enhanced Raman scattering enhancement factors: a comprehensive study," *J. Phys. Chem. C* **111**(37), 13794–13803 (2007).
57. H. Watanabe et al., "DFT vibrational calculations of Rhodamine 6G adsorbed on silver: analysis of tip-enhanced Raman spectroscopy," *J. Phys. Chem. B* **109**(11), 5012–5020 (2005).
58. S.-K. Park, N.-S. Lee, and S.-H. Lee, "Vibrational analysis of dopamine neutral base based on density functional force field," *Bull. Korean Chem. Soc.* **21**(10), 959–968 (2000).
59. W. R. Premasiri, R. H. Clarke, and M. E. Womble, "Urine analysis by laser Raman spectroscopy," *Lasers Surg. Med.* **28**(4), 330–334 (2001).

Ming Li received her PhD degree in mechanical/mechatronic engineering from University of Wollongong, Australia, in 2013. Since September 2013, she has been working as a postdoctoral research fellow at the Department of Electrical and Computer Engineering, University of Houston, USA. Her current research interests involve optofluidics, plasmonic biosensing, and MEMS.

Fusheng Zhao received BS degrees in electrical engineering from Tokyo Institute of Technology, Tokyo, Japan, in 2012. He joined Prof. W.-C. Shih's group in 2012 at the University of Houston and is currently a PhD candidate. His current research interests include nanoporous gold related nanofabrication and characterization. He is a member of SPIE and IEEE.

Jianbo Zeng received his PhD in analytical chemistry from Miami University in 2013. He joined in Prof. W.-C. Shih's group at University of Houston for postdoctoral training. His current research interest focuses on monolithic nanoporous plasmonic nanoparticles and their applications in optical sensors, catalysis, and nanomedicine.

Ji Qi received BS from Tsinghua University, Beijing, China, in 2008. She received her MS degree in University of Arizona, Tucson, AZ, in 2010. She joined Prof. W.-C. Shih's group in 2010 at University of Houston and is currently a PhD candidate. Her current research interests include innovative optical instrumentation, hyperspectral imaging, biosensing, spectroscopy, and plasmonics.

Jing Lu received her BS degree in electrical engineering from the University of Missouri, and BE degree in electronic information engineering from the University of Electronic Science and Technology of China in 2012.

Wei-Chuan Shih is an assistant professor of electrical and computer engineering and biomedical engineering at the University of Houston. He obtained a PhD from Massachusetts Institute of Technology under Michael S. Feld. He was an MIT Martin Fellow. He is a recipient of the NSF CAREER Award and NASA Early Career Faculty Grant. His research interests are nanobiophotonics, plasmonics, hyperspectral imaging, and N/MEMS. He is a member of OSA, IEEE, SPIE, SAS, and ASME.